Soil water dynamics affected by micro rainwater harvesting structures in Jordanian Badia restoration context

Coen Sprong

Universiteit Utrecht

ICARDA
Science for resilient livelihoods in dry areas

Soil water dynamics affected by micro rainwater harvesting structures in Jordanian Badia restoration context

MSc Thesis

06-2019

Author: Coen Hendrikus Cornelis Sprong

Student number: 4244648

E-mail: c.h.c.sprong@students.uu.nl

First supervisor: Geert Sterk

Co-supervisors: Stefan Strohmeier

Job de Vries

MSc Programme: Earth Surface and Water

Faculty of Geosciences

Department of Physical Geography

Utrecht University

Abstract

The objective of this study was to model and analyze the influence Vallerani rainwater harvesting (RWH) structures have on the soil moisture dynamics in the Jordanian Badia and to test viability of these structures when influenced by climate change. HYDRUS-2D was used for the modelling. A three-month fieldwork was performed to set up and calibrate the model. The results show that most of the soil moisture is located underneath the furrow of the Vallerani RWH structures. The impact on water availability is positive, almost halving the period of water stress. Climate change will have a big impact on the water availability provided by the Vallerani RWH structures. The most important factor of climate change on the viability of the Vallerani RWH structures is the rainfall intensity.

Table of Contents

List of figures

List of Tables

List of Appendices

1. Introduction

1.1 Background information

Water has been widely recognized as one of the most important natural resources (Vörösmarty et al., 2010; Dingman, 2015; Photo et al., 2018). On average the global annual renewable water supplies per capita are ∼ 7000 cubic meters (El Kharraz et al., 2012). Semi-arid and arid regions are characterized by low water availability. By definition these regions have a low amount of precipitation compared to the area's potential evapotranspiration. As a result of the limited water resources, the average annual per capita renewable water supply is lower than 1500 cubic meters, with Jordan facing a serious shortage with less than 230 cubic meters available per capita (El Kharraz et al., 2012). The limited water resources are the reason for the vulnerability of the ecosystems found in semi-arid and arid regions to changes in the water usage. Overexploitation of the natural resources may lead to land degradation, which includes the loss of the soil's ability to hold water required for vegetation growth (UNCCD, 2017). This land degradation process in semi-arid and arid regions is defined by the UNCCD as desertification.

A large semi-arid to arid region in the world is located in the Middle East and is locally known as "the Badia". The Badia used to refer to the region where the Bedouins live. It covers a major part of Jordan, approximately 72,600 square kilometers which is ∼81% of the country. On average the region experiences 50-150 mm of rainfall annually (Karrou et al., 2011). Even with its harsh conditions the Badia has been successfully inhabited for thousands of years. Since the 1960s the population density in the Badia has been increasing (Millington et al., 1999). This will continue to increase as a result of the ∼ 2% annual population growth that Jordan experiences and the political turmoil in the region. With this growth came a higher demand for meat, which in turn caused a surge in the amount of grazing animals. Because of this the grazing has exceeded the potential productivity of grazing resources (Karrou et al., 2011). This in combination with mismanagement of resources and removal of vegetation for fuel (Oweis et al., 2006) has caused desertification to occur in the Badia (Oweis et al., 2006; Karrou et al., 2011). With the mechanization of the agriculture in the region the process of desertification has accelerated and has become an even bigger problem (Oweis et al., 2006; Karrou et al., 2011).

Despite the water scarcity, agriculture is an important economic activity in the Badia. Most of the agriculture is rain-fed. However due to the low precipitation and limited water resources the agricultural yields are low and inconsistent (Oweis et al., 2006). To help with the cultivation of the land the people living in the Badia have been applying water harvesting techniques for over 9,000 years (Oweis et al., 2013). Rainwater harvesting (RWH) is a technique by which a part of the land is deprived of its share of rainwater and this rainwater is then added to another piece of land (Oweis et al., 2013).

This allows for the cultivation of a smaller section of the land. Rainwater harvesting can occur naturally in the form of a depression that fills with water during a rain shower or by human intervention. To accomplish the latter surface runoff has to be induced and redirected to the target area (Oweis et al., 2013). Water harvesting can be performed at both micro and macro scale. Water harvesting on micro scale usually covers areas of a few square meters and supports only a few plants. Macro scale water harvesting obtains its water from an entire watershed and is held within a reservoir.

1.2 Problem definition

In 1991 the food and agriculture organization of the United Nations (FAO) reported that the state of land degradation in Jordan is severe. They reported a great reduction in agricultural production of the land. To restore the productivity of the land it will require large scale and long term improvements (FAO, 2018). To combat the desertification that occurs in the Badia it is important to restore the vegetation growth in the region. Vegetation will protect the top soils from wind and water erosion (Oweis et al., 2006). To help with this, new water harvesting techniques have been developed. Italian agronomist Venanzio Vallerani designed two ploughs that can be used to build contour ridges and semi-circular rain water harvesting (RWH) catchments. These ploughs can be used to create up to 7,500 micro-catchments per day (Ali et al., 2006). This method of micro water harvesting could be part of the solution to the problems in the Badia and help restore the land (Ali et al., 2006).
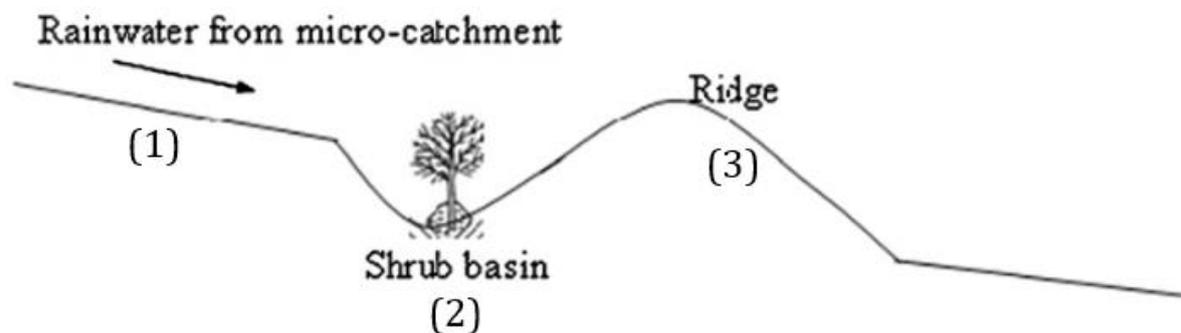
Figure 1 A schematic overview of a micro rainwater harvesting structure. (Taken from Ali et al., 2010)

The structures created by the Vallerani ploughs (Vallerani RWH structures) are considered micro water harvesting structures. A Vallerani RWH structure consists of three segments (Fig. 1): (1) a slope, (2) a furrow or shrub basin and (3) a ridge. Due to a poor soil structure and low vegetation cover in arid regions soil surface crusting occurs. As a result of this crusting, surface runoff is generated on the slope even during small rain showers (Ali et al., 2010). This surface runoff generated on the slope is directed into the furrow. Within these furrows either seeds or seedlings are planted (Ali et al., 2006). The theory is that at the start the plants can establish themselves and over time the furrow will be filled up and its efficiency will drop. However, at that time the plants are

strong enough to survive without the support of the structure. The ridge is created to catch all the surface runoff that is generated during the rain showers.

Since the development of the Vallerani technique in 1988 it has been tested in at least ten different countries. The tests in these countries have been met with success (Malagnoux, 2008). Using this technique, the survival rates of the shrubs increased from 16% to 100% (Karrou et al., 2011). The implementation of the RWH structures positively influenced the water productivity of the shrubs growing within the structures (Mudabber et al., 2011). This increased water productivity varies with the wetness of the year, having the largest impact for dry years (Akroush et al., 2011). Moreover, Akroush et al. (2011) observed a steady increase in the soils organic matter percentage after implementation.

The vast majority of the studies put their focus on the most efficient ways to construct Vallerani RWH structures throughout the landscape and its direct impact on the shrubs (Ali et al., 2006; Ali et al., 2007; Malagnoux, 2008; Ali et al., 2010; Akroush et al., 2011; Mudabber et al., 2011; Karrou et al., 2011; Ziadat et al., 2012). However, almost no research has been performed on the soil moisture dynamics around a Vallerani RWH structure over a longer period of time. Likely, no attempts have been done to model the influence on soil moisture of the Vallerani RWH structures. In the future the hydrology of the Badia may be altered as a result of climate change. It is predicted that by the year 2100 the annual precipitation will be ~20% lower but with a higher intensity and the temperatures will be 3,5°C higher (Kunstmann et al., 2007; Evans, 2009; Lelieveld et al., 2012). This climate change could have an impact on the water retention capacity of the Vallerani RWH structures. No studies have been performed to the potential impact of climate change on the effectiveness of the Vallerani RWH structures.

1.3 Study objectives

With the increasing pressure on the rangelands in the Badia comes an increase in importance of water harvesting practices to enhance the resilience of the ecosystem and to support both the agriculture and the livestock feed provision. The Vallerani RWH structures have been widely tested for its effects on agriculture and to find the most efficient placement. However, there is a significant knowledge gap on their influence on soil moisture dynamics and the potential impacts of climate change on the Vallerani RWH structures. The aim of this study was to set up a model which can successfully simulate and quantify the Vallerani RWH structures and their influence on the soil moisture dynamics. For this purpose, the HYDRUS 2D model was used. After calibrating the model using field observations it was applied to simulate the different climate change scenarios. This was done to test the water retention capacity of the Vallerani RWH structures now and in the future. The results will be part of a larger holistic research focussing on assessment of water harvesting on a landscape scale.

The study objectives can be summarized as:

- To quantify the soil moisture dynamics in the field in and around the Vallerani structures on a high spatial and temporal resolution

- Model the soil moisture dynamics using Hydrus-2D

- Evaluate the water retention capacity of the Vallerani structures throughout different climate change scenarios

2. Study area

This research focusses on a single watershed located in the Badia in Jordan (Fig. 2). The watershed is located 30 kilometers southeast of the capital of Jordan (Amman). It is located nearby two communities that live in the Badia, the Mharib and the Majedieh (Ali et al., 2006). These communities have populations of 300 and 120 people respectively (Karrou et al., 2011). The main land use is barley production and rangeland. The site has an altitude ranging from 820 to 846 meters (Karrou et al., 2011). 80% of the land in the area is private land, 15% is owned by the government, and 5% is owned by people outside the community. The average holding is 7.5 ha (Karrou et al., 2011).

A Vallerani plough was used to create RWH structures over circa 14.7 ha of the test site (Fig. 3). They are constructed along the contour of the slope with a spacing of 6 to 9 m. The lengths of the structures are on average

Figure 2 Satellite imagery of the study region. Green outline is the country of Jordan. Red outline is the study area and is enlarged in the inset. Blue outline is the watershed containing Vallerani RWH structures.

4.0 to 4.5 m and the ridge and furrow both have a width of circa 0.5 m. Within the furrow seedlings of the Atriplex Halimus shrub were planted. This shrub is used as food for the local livestock. It has a water stress level of -3.5 MPa (pF of 4.54) (Martìnez et al., 2003; Belkheiri and Maurizio, 2013).

Figure 3 Left: the plow used to create the Vallerani RWH structures. Right: the landscape with the Vallerani RWH structures.

Because of the watershed's location in the Badia it experiences a Mediterranean semi-arid to arid climate (Karrou et al., 2011). The amount of annual rainfall is low with less than 150 mm on average per year. The rainfall is erratic in distribution throughout the year and between years (Karrou et al., 2011). Most of the rain falls during intensive showers. The rainy season in the area is from September till May. However, the majority of the rainfall happens from December till March (Karrou et al., 2011). Most of the natural vegetation are shrubs which are present for ~3 months of the year. However, only a small amount of these shrubs remain. Because of this, nomadic communities have to travel long distances to feed their flocks (Ali et al., 2006). Barley is the main crop that is produced in the Badia (Karrou et al., 2011). 70% of the Jordan livestock comes from the Badia (Oweis et al., 2006).

The soils in the Badia are heterogeneous. Rawajfih et al. (2005) analysed the soil type north of the study area. They found that along a short distance the soil type is variable. The soils in the Badia are rich in silt and calcium (Karrou et al., 2011). According to Rawajfih et al. (2005) the top parts of the soil contain atleast 30% silt. When it is dry the soil is moderately hard. The stone and gravel content of the soil is high and when the soil is tilled the gravel and stones come to the surface (Karrou et al., 2011). There are three soil textures that are dominant in the study area (Karrou et al., 2011):

- Silty clay loam
- Silty clay
- Silty loam

Fieldwork performed by the National Agricultural Research Center of Jordan (NARC) confirmed the findings by Karrou et al. 2011 for the study area.

In large parts of the study area a crust is formed on the surface of the soil, which reduces the infiltration rate and stimulates surface runoff generation (Karrou et al., 2011). The permeability of the soil is moderate with a low amount of structures within the soil (Ali et al., 2006). The high erodibility of the soil is indicated by the amount of gullies found in the area (Ali et al., 2006; Karrou et al., 2011).

3. Methods

3.1 Model description

In this research the HYDRUS 2D model was applied. HYDRUS 2D is a finite element model that can be used to simulate two-dimensional movement of water, heat and solutes. For the movement of water in saturated and unsaturated soils HYDRUS 2D numerically solves the Richards equation.

3.1.1 Uniform flow

The Richards equation (Eq. 1.) is used to describe the uniform variably-saturated water flow in HYDRUS 2D (Šimůnek et al., 2008).

$$\frac{\partial \theta(h)}{\partial t} = \frac{\partial}{\partial x_i}\left[K(h)\left(K_{ij}^A \frac{\partial h}{\partial x_j} + K_{iz}^A \right)\right] - S(h) \tag{1}$$

In this equation θ is the volumetric water content [$L^3 L^{-3}$]; h is the pressure head [L]; K is the unsaturated hydraulic conductivity [LT^{-1}]; K^A_{ij} and K^A_{iz} are the components of a dimensionless anisotropy tensor K^A; S is the general sink/source term [$L^3 L^{-3}T^{-1}$] which accounts for root water uptake; t is the time [T]; and x_i and x_j are the spatial coordinates [L] (Šimůnek et al., 2008).

Due to the strong nonlinear nature of the Richards equation it is only possible to derive a few simplified analytical solutions. Most practical applications of the equation require numerical solutions. These solutions can be obtained using the finite differences or finite elements methods. To solve equation 1, knowledge of the soil water retention and hydraulic conductivity are required. HYDRUS 2D uses the analytical models for the hydraulic conductivity as described in Šimůnek et al. (2008). The Richards equation is inversely related to the resistance to water flow because it contains the hydraulic conductivity. HYDRUS 2D applies the analytical models described in Šimůnek et al. (2008) based on the relation between the Richards equation and resistance to water flow.

3.1.2 Soil Hydraulic Model

For this study the van Genuchten-Mualem model was used (van Genuchten, 1980). This model contains a simple equation that allows for estimations of the soil moisture retention data. The model applies the hydraulic conductivity using the model proposed by Mualem (1976). This model requires multiple parameters for its calculations (Table 1) these parameters will henceforth be referred to as the Van Genuchten parameters, which will be estimated using the Rosetta procedure (See 3.1.5)

Table 1 Overview of the van Genuchten parameters.

Parameter	Unit	Definition
Q_r	cm^3/cm^3	Residual water content
Q_s	cm^3/cm^3	Saturated water content
K_s	cm/day	Hydraulic conductivity
n	(-)	Van Genuchten curve fitting parameter
Alpha	cm^{-1}	Van Genuchten curve fitting parameter
I	(-)	Pore-connectivity parameter

3.1.3 Root water uptake

For this study an S-shaped water stress response function was applied as suggested by van Genuchten (1985). This requires two input parameters: the pressure head at which root water uptake is reduced by 50% and the pressure head at the wilting point.

Slatyer (1970) found transpiration values for two species of Atriplex, one of these species is closely related to Atriplex Halimus. These values were taken for the calculations of the transpiration rate in the model.

3.1.4 Inverse parameter estimation

HYDRUS 2D has the option of inversely solving the equations. By doing this measured soil moisture data can be used as input for the model and it will estimate the remaining Van Genuchten parameters (Table 1) (Šimůnek et al., 2008). HYDRUS 2D uses the parameter estimation technique of Marquardt-Levenberg as discussed in Šimůnek and Hopmans (2002). This method is used to find parameters for both soil hydraulic (Šimůnek et al., 2002) and solute transport parameters (Hopmans et al., 2002).

3.1.5 Rosetta parameter estimation

Due to the importance of the soil hydraulic properties HYDRUS 2D contains Rosetta Lite v1.1. Rosetta is a model that predicts the Van Genuchten parameters based on sand, silt and clay percentages and the bulk density of the soil. These predictions are made by the implementation of five hierarchical pedotransfer functions. These pedotransfer functions are based on soil data that is readily available. The creation of the Rosetta model used data obtained from pedogenic processes of temperate climates in North America and Europe. A more detailed overview into the working of the Rosetta model can be found in Schaap et al. (1998) and Schaap et al. (2001)

3.2 Model application

The soil moisture dynamics were modelled across a single Vallerani RWH structure. To obtain all the Van Genuchten parameters two parameter estimation techniques were

tested. First inverse parameter estimation was performed but results were deemed unreliable (Appendix A).

The second method used was the Rosetta parameter estimation. This was used to obtain five different sets of parameters. Using these parameter sets the model was run for 162 days. The model results were evaluated to find the best parameter set.

Using the best evaluated parameter set four different scenarios were modelled. These scenarios covered an entire year running from the 10th of October 2017 till the 9th of October 2018. First the present day conditions were modelled for this time period. Three different climate change scenarios were modelled by altering the present day climate conditions for the time period.

3.3 Model input

The Rosetta model requires soil texture and bulk density per soil layer to estimate the Van Genuchten parameters. For this study the soil was divided into two layers. Data of the soil textures was obtained from NARC.

The Van Genuchten parameters are important HYDRUS 2D input parameters. Four more variables are important input for HYDRUS 2D. These are: water level within the Vallerani RWH structure, precipitation, evaporation and transpiration.

Field measurements were performed to obtain these variables. Precipitation, infiltration and temperature measurements were performed during fieldwork. This fieldwork took place from November 2018 until February 2019. Soil microtopography and slope were measured to get an accurate representation of the structure within HYDRUS 2D. The measurements took place over multiple Vallerani RWH structures that are all located on a single hillslope (Fig. 4 & Fig. 5).
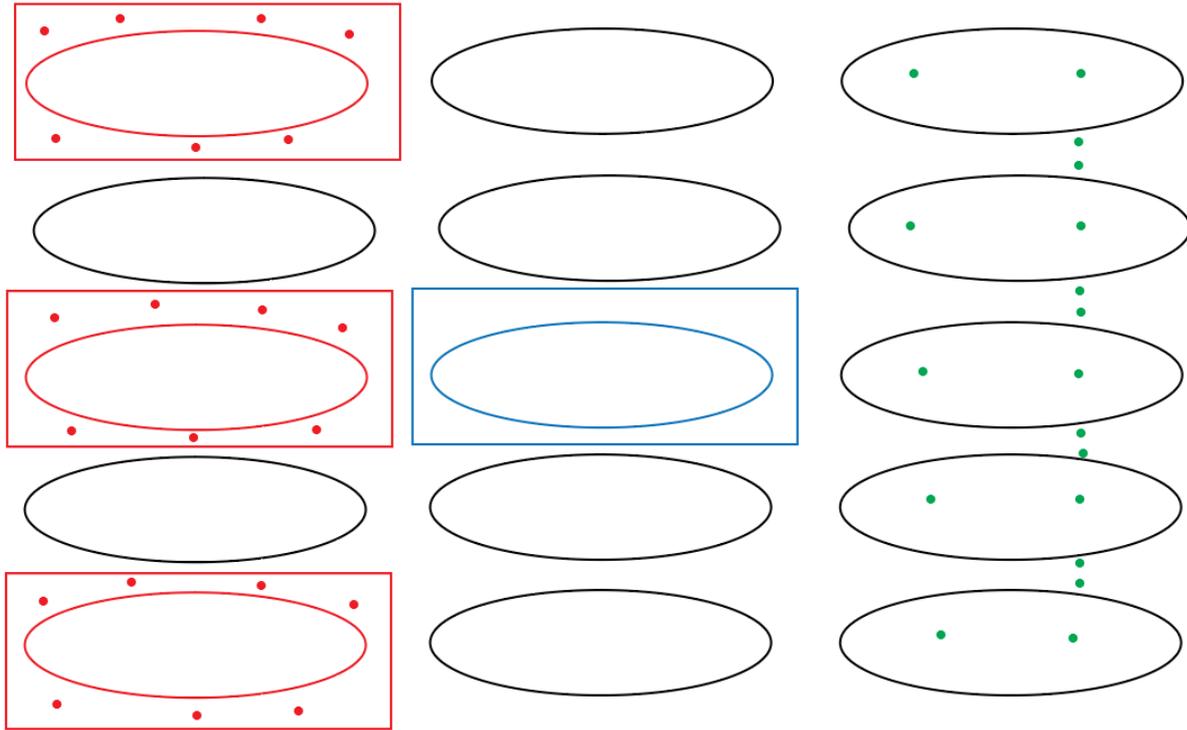
Figure 5 Schematic overview of the hillslope on which the experiments took place. In red the Vallerani RWH structures a long which photogrammetry was performed. Blue outline is the structure around which the Decagon 5TE sensors were installed (Figure 9 for detailed placement). Green dots are the TRIME-PICO sensors.

Figure 4 The hillslope where the Vallerani RWH structures were created on which the experiments were performed.

3.3.1 Water level

The water levels in the Vallerani RWH structure are a combination of the surface runoff, precipitation, evaporation and infiltration. The structure shape obtained from photogrammetry (See 3.3.4) was used to create a fill curve. With this curve increases in water level were calculated based on the surface runoff data. Equation 2 is the equation used to calculated the water level in the next time step.

$$W_t = W_{t-1} + R + P - I - E \qquad (2)$$

In this equation W is the water level at timestep t (cm), R is the rise in water level due to surface runoff (cm), P is the amount of precipitation (cm), *I* is the amount of infiltration (cm) and E is the evaporation (cm).

3.3.1.1 Surface Runoff

For the study area the Rangeland Hydrology and Erosion Model (RHEM) has been constructed (Haddad, 2019). Based on the results of RHEM, surface runoff values were calculated for this study. Based on close by surface runoff plot experiments, if precipitation was at least 5mm/day surface runoff was induced with a factor of 0.3. If the intensity was more than 10mm/day the surface runoff was induced with a factor of 0.4 (Strohmeier, 2019). For the climate scenarios surface runoff was calculated using the same methodology.

3.3.1.2 Infiltration rate

Infiltration rates were measured with two different methods: the double-ring infiltrometer (Fig. 6) and forced infiltration (Fig. 7).

Figure 6 Test site set up of the double-ring infiltrometer. Inside the furrow (right) and on the hillslope (left).

For the double-ring infiltrometer experiments both rings were placed into the soil and filled with water. The bigger ring was filled with 8 centimeters of water. This was done to negate lateral flow out of the small ring. The small ring was filled with 5 centimeters of water. This water level was measured every 5 minutes and then refilled to 5 centimeters. The experiment was stopped once the infiltration rate was found to be constant over multiple measurements. This experiment was performed three times on

three separate locations: inside the Vallerani RWH structure, once just upstream of the furrow and the third time on the slope in between two structures.

For the forced infiltration experiment the Vallerani RWH structure in which the Decagon 5TE sensors were installed was filled with water till its maximum capacity (Fig. 7). Once the structure was completely filled the water level was measured in the centre of the structure. After this, water level measurements were taken every five minutes for the initial twenty minutes. The rest of the first hour measurements were taken every ten minutes and after this, measurements were taken every half hour until all of the water had infiltrated. The same experiment was performed on a second Vallerani RWH structure next to the first structure.

Figure 7 The forced infiltration experiment performed in the field.

3.3.2 Precipitation
The precipitation is used in the HYDRUS 2D model twice. It is used for the calculations of the water level and for the amount of water the slope receives. Within the study area the rainfall was measured using a tipping bucket rain gauge. The rain gauge has a registration interval of five minutes.

3.3.3 Potential evapotranspiration
HYDRUS 2D uses the potential evapotranspiration to calculate the amount of water that will evaporate and how much will infiltrate into the soil. In dry periods it will account for the drying of the soil. In this study the Thornthwaite temperature based model was used to calculate the potential evapotranspiration (Eq. 3,4,5) (Dingman, 2015).

$$PET = 16 * \left(\frac{L}{12}\right) * \left(\frac{N}{30}\right) * \left(\frac{10T_d}{I}\right)^{\alpha} \tag{3}$$

PET is the estimated potential evapotranspiration (mm/month), T_d is the daily average temperature (°C), N is the number of days in the month, L is the average length of daytime (hours), α is obtained through equation 4.

$$\alpha = (6.75 * 10^{-7})I^3 - (7.71 * 10^{-5})I^2 + (1.792 * 10^{-2})I + 0.49239 \quad (4)$$

I is the heat index calculated using equation 5.

$$I = \sum_{i=1}^{12} (\frac{T_{mi}}{5})^{1.514} \qquad\qquad\qquad (5)$$

T_{mi} is the mean monthly temperature (°C).

The heat index was calculated using average temperature data from the Queen Alia airport. This dataset spans ~30 years and the airport is located near the study area.

3.3.4 Soil microtopography and slope
The soil microtopography and slope are important for HYDRUS 2D. They provide the shape of the surface the model performs the calculations over. It was also required to create a fill curve of the furrow for the calculations of the water level.

Close-range photogrammetry was used to get an accurate soil microtopography and slope of the Vallerani RWH structures. Along the structures seven distinguishable markers were placed (Fig. 4) (Strohmeier at al., 2018). These were used for the ground truthing and stitching of the photos. Around the Vallerani RWH structure photos were taken including at least two of the markers (Fig. 8). A more extensive explanation of the photogrammetry

Figure 8 Photogrammetry being performed in the field.

process can be found in Appendix B. The photogrammetry process resulted in a 3D model of the surface. From this 3D model accurate surface profiles were exported to HYDRUS 2D. These profiles allowed for modelling over a surface that is a close representation of reality. The slopes HYDRUS 2D requires for its modelling were also obtained from the surface profiles.

3.3.5 Soil texture
The National Agricultural Research Centre of Jordan (NARC) performed fieldwork in the same study area in 2017. NARC performed soil sampling throughout the study area at ten different locations. Based on this fieldwork data, four sets of soil texture were created (Table 2). The sets vary in sampling locations.

Table 2 Overview of the soil percentages for each of the four sets.

Set	Sand (%)	Silt (%)	Clay (%)
1	16.8	44.9	38.0
2_{top}	19.5	45.3	35.3
2_{deep}	13.2	46.4	40.6
3_{top}	24.9	43.7	31.5
3_{deep}	10.5	49.5	40.9
4_{top}	20.4	48.0	31.7
4_{deep}	13.3	46.2	39.7

3.4 Model evaluation

To evaluate the model results soil moisture measurements were taken in the field using soil moisture sensors. The soil moisture sensors installed for this research are Decagon 5TE, Frequency-Domain sensors. The Decagon 5TE are relatively simple sensors with some flaws. An extensive discussion on the sensors can be found in Chavez & Evett (2012) and in Singh et al. (2018). Advantages of the sensor are the short measurement interval and its longevity allowing for continued measuring over a longer period of time. According to the user manual provided by the manufacturer the measurement error of the sensors should be ~3%.
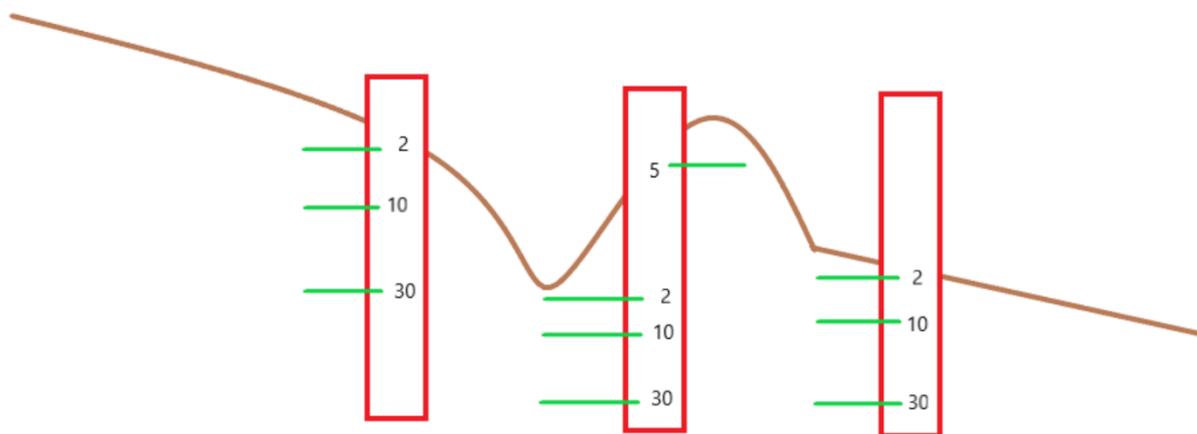
Figure 9 Schematic overview of the Decagon 5TE sensor placement along the Vallerani RWH structure. Depths are in centimeters below surface.

Along a single Vallerani structure a network of Decagon 5TE sensors was set up. Ten sensors were installed along the structure at various depths. Three sensors were installed directly underneath the furrow, three sensors were installed half a meter upstream of the furrow and three downstream of the furrow. The last sensor was placed

inside the ridge. Figure 9 gives a schematic overview of the sensor placement along the Vallerani RWH structure.

To install the sensors, cuts were made into the Vallerani RWH structure (Fig. 10). These cuts were made in a way to prevent altering the water dynamics of the structures as much as possible. After the sensors were installed the cuts were filled up to represent the original state as much as possible (Fig. 10).

In December 2017 38 TRIME-PICO sensors were installed along a transect of Vallerani RWH structures (Fig. 4). These are Time-Domain reflectometry sensors. To read out the sensors, access tubes were dug and installed along the transect. A detailed explanation on the installation of these sensors can be found in Fukai (2019).

Two sets of soil moisture measurements were used for this research. The oldest dataset provides soil moisture data since December 2017 and is produced by the TRIME-PICO sensors. The second dataset is based on the Decagon 5TE sensors that were installed in December 2018 and started recording on the 18th of December. Both of these datasets were used for validation.

For each set of Van Genuchten parameters the model was used to calculate the soil moisture in the system. This was done for a period from the 10th of October 2017 till the 9th of October 2018. Which resulted in a total of 5 model runs.

Figure 10 Left: Picture of the cut used to install the Decagon 5TE sensors. Right: The Vallerani RWH structure after the cut was filled up.

Using the measured soil moisture datasets, the goodness-of-fit (GOF) of the model runs was evaluated. Three different GOF parameters were used for this evaluation: Bias, Correlation and the Kling-Gupta efficiency. The Kling-Gupta efficiency takes the correlation, bias and variability into account while also testing the relative importance of

these three different factors. An elaborate explanation of the Kling-Gupta efficiency and its advantages can be found in Gupta et al. (2009) and Kling et al (2012).

3.5 Climate scenarios

To test the water retention capacity of the Vallerani RWH structures in the future, three different climate scenarios were modelled. These scenarios were modelled using altered precipitation and temperature data. The climate scenarios range from minimal to maximum climate change. The climate change prognosis for the Badia region is a decrease in precipitation of roughly 20%, an increase in precipitation intensity and an increase in temperature of ~3.5°C by the year 2100 (Kunstmann et al., 2007; Evans, 2009; Lelieveld et al., 2012). To realistically increase the rainfall intensity, current rainfall data was analysed and divided into three classes: small, medium and heavy rain events. To increase intensity for the climate scenarios small and medium rain events were altered to become medium and heavy rain events, respectively.

For the first scenario the precipitation was reduced by 10% and the temperature increased by 1.2°C, but for this event the rainfall intensity was not altered. For the second scenario the rainfall was reduced by 20% and the temperature increased by 2.5°C. To increase the rain intensity, the small rain events were combined to create more intense rain events. For the third scenario the precipitation was reduced by 30% and the temperature increased by 3.5°C. To increase the rainfall intensity, the smallest rain events were removed and the smaller rain events were increased to turn them into heavy rain events. A summary of the scenarios is given in table 3.

Table 3 Summary of the climate scenario settings.

Scenario	Rainfall amount	Temperature change	Intensity changes
	%	°C	
1	-10	+1.2	None
2	-20	+2.5	Smallest events combined into more intense events
3	-30	+3.5	Smallest events removed. small events made into heavy events.

4. Results

4.1 Surface profile & Surface runoff water level increase

A total of 373 photos were used to generate an accurate Digital Elevation Model (DEM) of the Vallerani RWH structure. A 2D surface profile through the center of the structure was obtained from the DEM. An accurate fill curve was created to calculate the increase in water height per volume of water.

Throughout the model period surface runoff occurred on six occasions. The magnitude of these events ranges from 1 – 10mm. The slope length along which the surface runoff is induced is 7 meters. Table 4 gives an overview of the dates and increases in water level. If the increase in water level was higher than the Vallerani RWH structure's maximum capacity the water was removed from the system.

Table 4 Overview of the surface runoff events with the water level increases.

Date	Water level increase *(cm)*
25-12-2017	6.8
05-01-2018	12.2
19-01-2018	17.3
13-02-2018	10.0
17-02-2018	6.5
26-04-2018	4.4

4.2 Infiltration rates

The double-ring infiltrometer tests were performed on the 24th of January 2019. On average it took 90 minutes per experiment before the infiltration rates remained constant. Strong winds influenced the surface of the water within the first ring. Within the Vallerani RWH structure the final infiltration rate was 24 mm/hour. It was 42mm/hour just upstream of the furrow and 33mm/hour on the slope in between two structures.

The Vallerani RWH structures were filled with water on the 22nd of January 2019. The maximum water height in the structure with the Decagon 5TE sensors was 14.1 centimeters. This is a volume of ~260 liters of water. It took roughly three hours for all the water to infiltrate, which is equal to an average infiltration rate of 47mm/hour. The second structure that was filled had a maximum water height of 12.2 centimeters and a volume of ~160 liters. The infiltration time of this structure was the same. The initial infiltration rates over the first five minutes of the experiments were 240mm/hour and 252mm/hour. This high rate dropped off quickly, after 15 minutes they were 114mm/hour and 120mm/hour respectively. After two and a half hours the rate was only 20mm/hour for both structures. At this point the remaining water height was ~5 millimeters.

The lowering of the water level in both of the Vallerani RWH structures follows a similar pattern (Fig. 11). The amount of infiltrated water can be calculated as follows:

$$WH = 152.26e^{-0.023t} \tag{6}$$

For the Vallerani RWH structure with the Decagon 5TE sensors. The water level in the 2nd Vallerani RWH structure can be calculated as:

$$WH = 112.5e^{-0.022t} \tag{7}$$

The goodness of fit (R^2) parameter is 0.96 for both of the fitted curves.
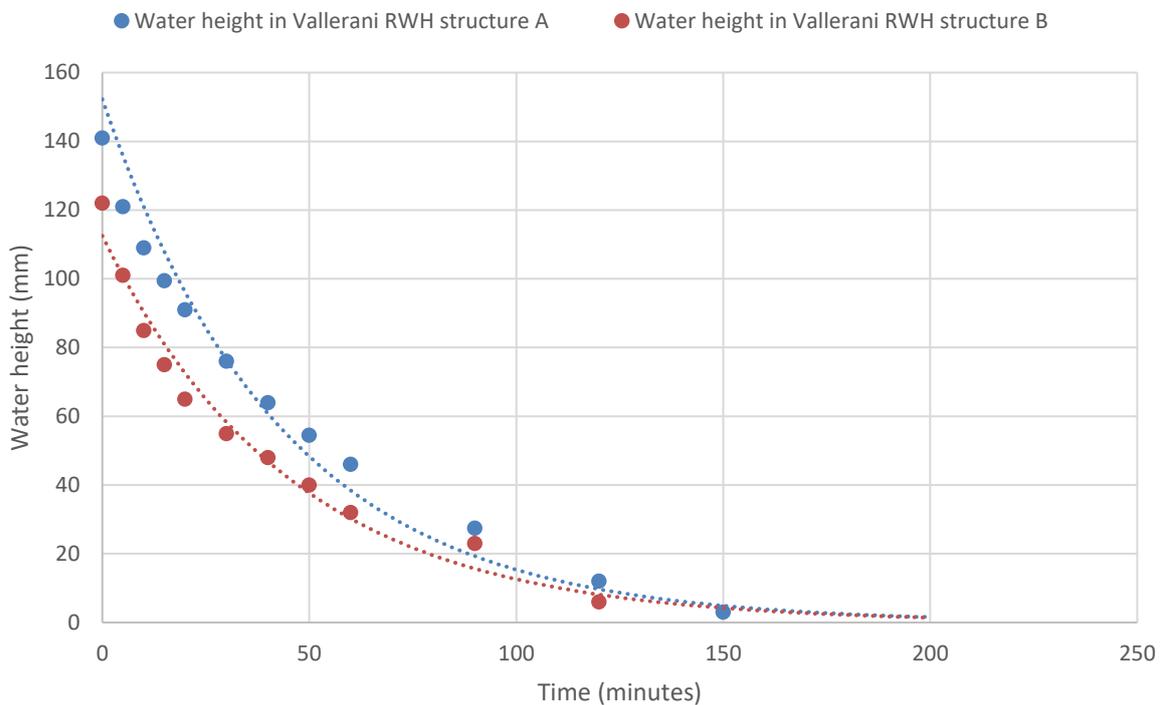
Figure 11 Water height over time in two Vallerani RWH structures during the fill experiments. Structure A is the Vallerani RWH structure containing the Decagon 5TE sensors. Structure B is the second Vallerani RWH structure that was filled.

4.3 Soil moisture

4.3.1 Decagon 5TE sensors

The Decagon 5TE sensors were installed on the 18th of December 2018. The last read out of the sensors was performed on the 6th of March 2019. Figures 12, 13 and 14 show the soil moisture data measured by the Decagon 5TE sensors plotted with the measured precipitation data. During this measurement period four rainfall events occurred that were large enough to induce runoff. The measured soil moisture data should have been clearly affected by the four runoff events and the infiltration test.

The sensors directly underneath the furrow were the only sensors that were affected by the five events (Fig. 12). Overall the sensors underneath the furrow measured the lowest soil moisture values. These sensors should have measured the highest values. The

sensor at a depth of 10cm measured values lower than both the sensors above it and underneath it.
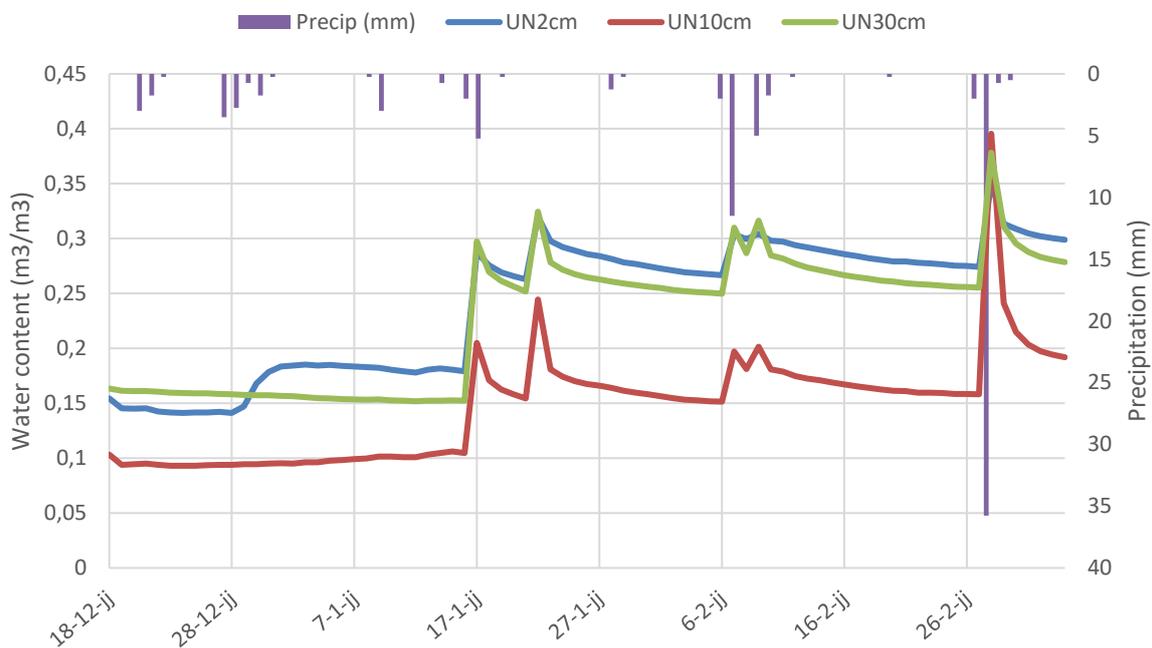
Figure 12 Soil moisture measurements obtained from Decagon 5TE sensors at depths of 2 cm, 10 cm and 30 cm underneath the furrow of a Vallerani RWH structure from the 18th of December 2018 till the 6th of March 2019. Measured precipitation values for the same period on the secondary axis.

The Decagon 5TE sensors downstream of the furrow (Fig. 13) were not affected by the five events. They measured very little response throughout the entire measurement period. The peaks in the measurements were not in line with the timing of the rainfall events. At the end of the measurement period the sensors measure values up to 63% water content.
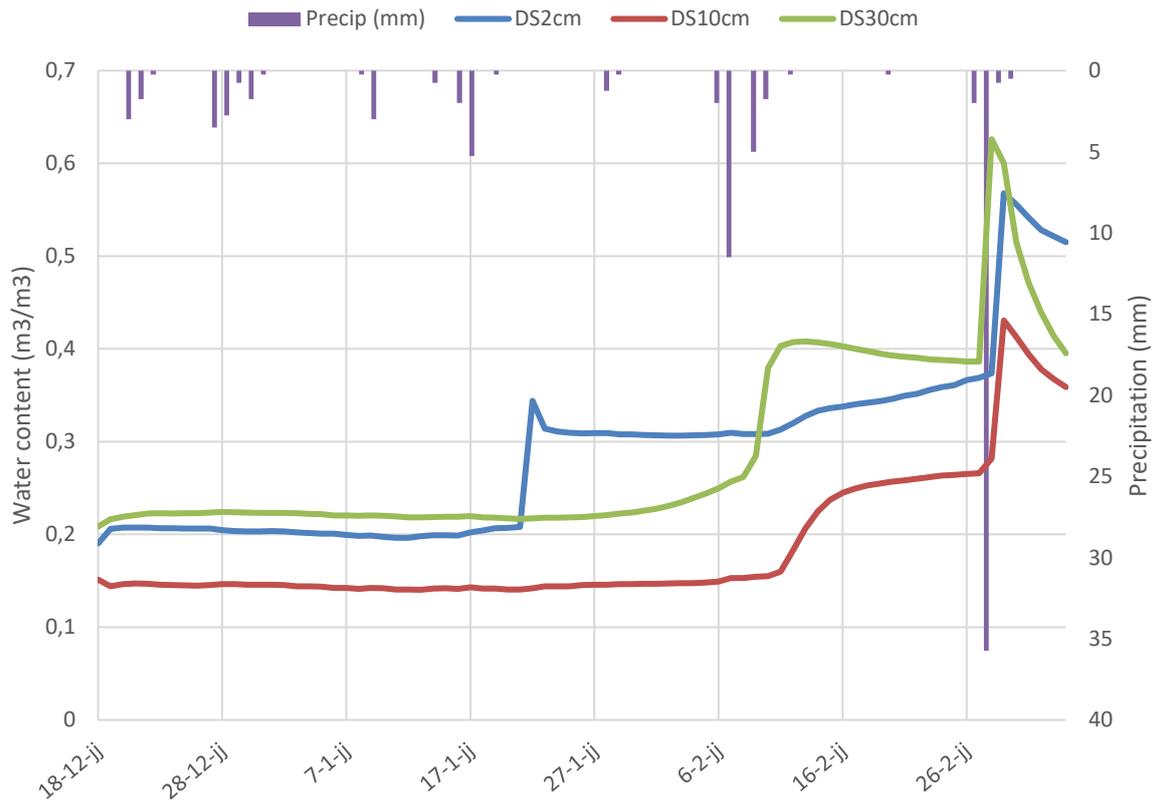
Figure 13 Soil moisture measurements obtained from Decagon 5TE sensors at depths of 2 cm, 10 cm and 30 cm downstream of the furrow of a Vallerani RWH structure from the 18th of December 2018 till the 6th of March 2019. Measured precipitation values for the same period on the secondary axis.

Upstream of the furrow the Decagon 5TE sensors registered a chaotic pattern (Fig. 14). Small rainfall events triggered a response from the sensors. On multiple occasions throughout the measurement period measured water content is more than 50%.
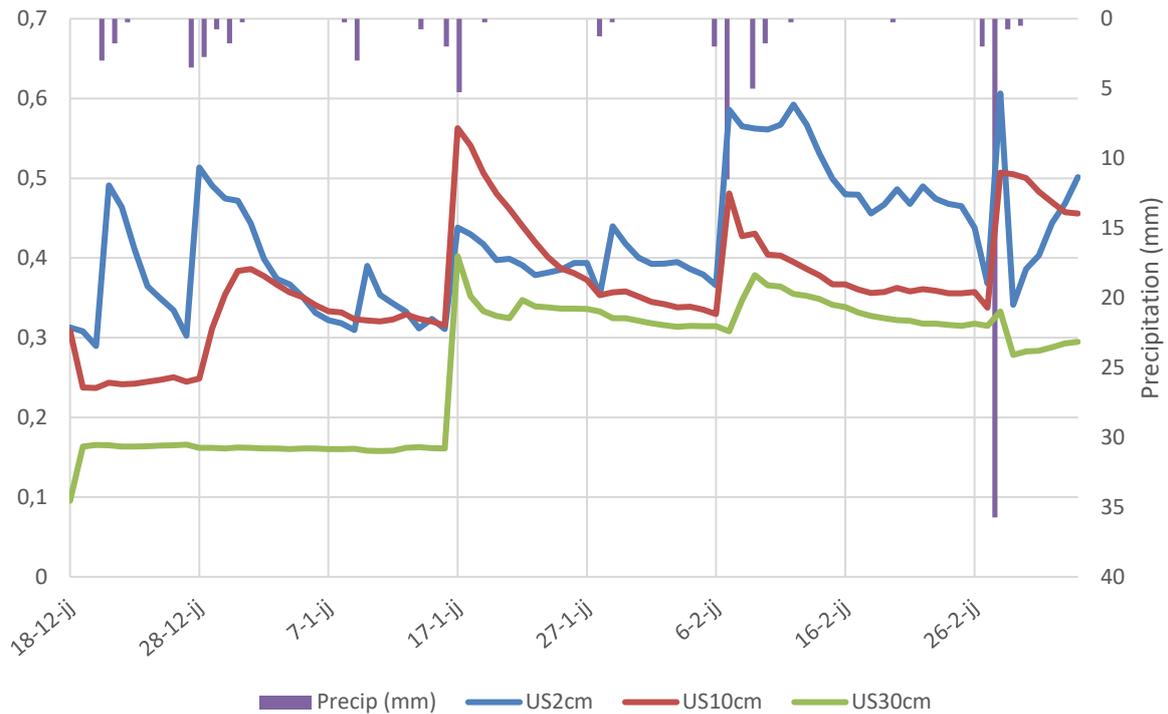
Figure 14 Soil moisture measurements obtained from Decagon 5TE sensors at depths of 2 cm, 10 cm and 30 cm upstream of the furrow of a Vallerani RWH structure. From the 18th of December 2018 till the 6th of March 2019. Measured precipitation values for the same period on the secondary axis.

Overall the values measured by the Decagon 5TE are not in line with the expected values. Measuring the lowest water content values in the wettest region of the system. The measured values also went above the expected maximum water content on multiple occasions.

4.3.2 TRIME-PICO sensors

Six TRIME-PICO were deemed suitable for this study. These sensors were installed upstream, downstream and underneath the furrow of a Vallerani RWH structure at depths of 10 and 30 centimeters. The measurements were taken over the period from the 19th of Decembers 2017 till the 10th of May 2018. On average there is one measurement available per week (Fig. 15).

The values measured by the TRIME-PICO sensor were in line with was expected of the soil moisture. Directly underneath the furrow the values were the highest. Upstream and downstream there is only a response when a larger rainfall event occurred (Fig. 15).
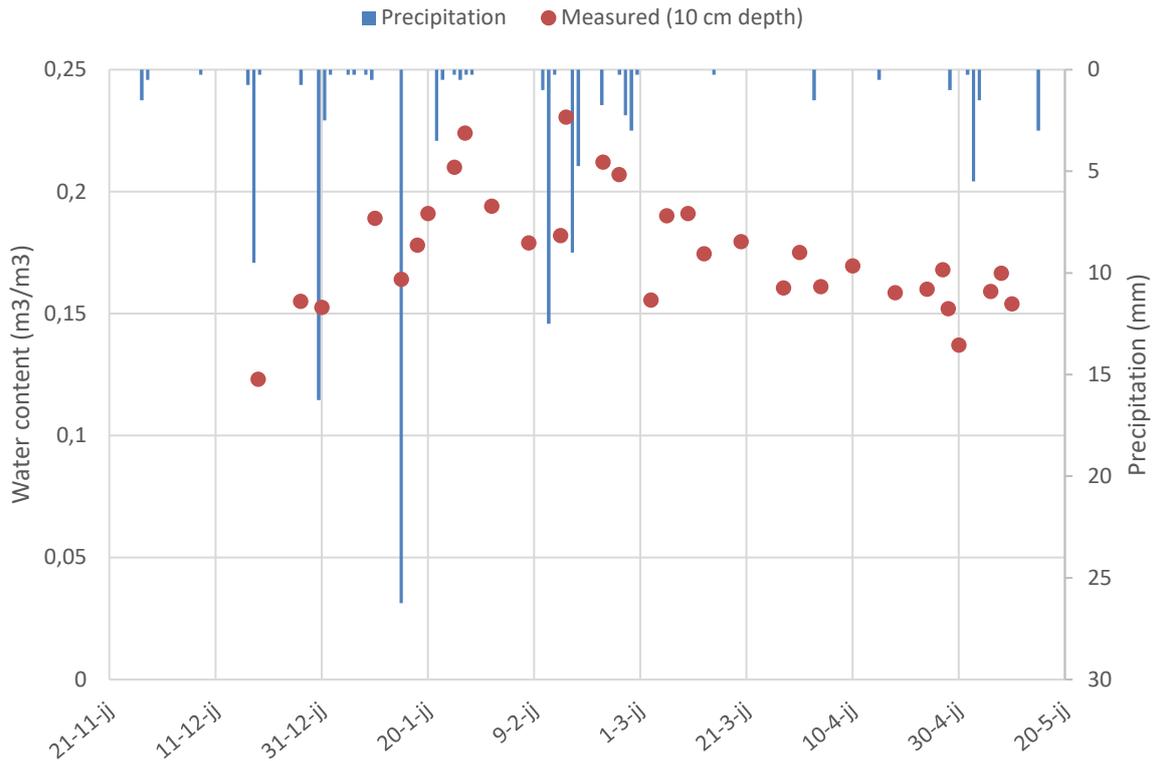
Figure 15 Soil moisture measurements values obtained from the TRIME-PICO sensor at a depth of 10 cm upstream of the furrow of a Vallerani RWH structure from the 19th of December 2017 till the 10th of May 2018. Measured precipitation values from the 21st of November 2017 till the 20th of May 2018 on the secondary axis.

4.4 Model evaluation

Five set of Van Genuchten parameters were obtained using the Rosetta parameter estimation. Due to the poor performance of the Decagon 5TE sensors they were not used for the model evaluation. Instead the measurements of the TRIME-PICO sensors were used. The model runs were performed over the time period from 1st of December 2017 till the 20th of May 2018. The model runs were evaluated with all the TRIME-PICO measurements available for this time period.

Table 5 gives an overview of the GOF of the five model runs. The first four sets of parameters show similar GOF results. All of these sets overestimated the soil moisture upstream and downstream of the Vallerani RWH structure. Parameter set 5 did not overestimate this, which increased the GOF.

Table 5 Goodness-of-fit results for the Rosetta modelling.

Parameter set	Correlation	Bias	Kling-Gupta Efficiency
	(-)	*(%)*	*(-)*
1	0.50	18.20	0.42
2	0.49	14.00	0.40
3	0.44	10.20	0.34
4	0.46	8.90	0.35
5	0.73	-2.00	0.55

4.4.1 Model run 5

Parameter set five gave the best results (Appendix C). Upstream at a depth of 10 cm the magnitude of both measured and modelled values are equal (Fig. 16). The modelled values have higher peaks than are measured but due to the irregular measurement interval the peaks might not have been measured. On average the measured values are ~1% higher than the modelled values. At a depth of 30 cm the modelled values are higher than the measured values (Fig. 16). Only seven measured values are higher than the modelled values. In the first half of the period the model peaks multiple times. These peaks are not as visible in the measured values. In the second half the modelled values show a steady decline while the measured values increase on multiple occasions.
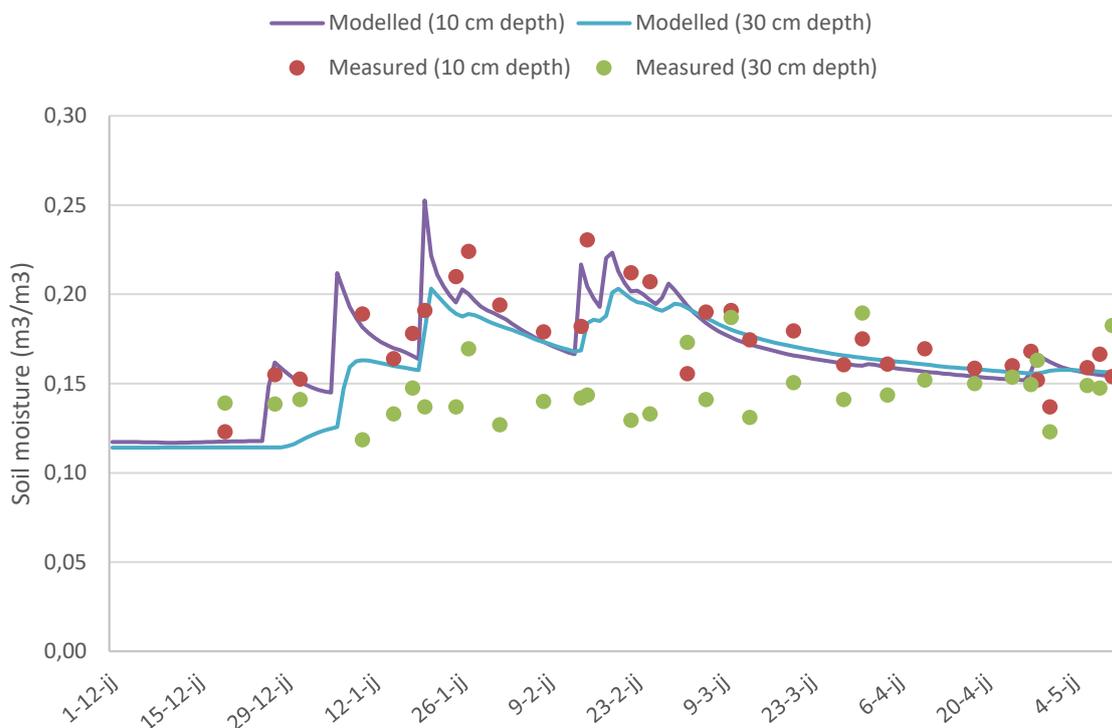
Figure 16 Modelled and measured soil moisture values upstream of the Vallerani RWH structure at depths of 10cm and 30cm for a period from the 1st of December 2017 till the 5th of May 2018. Measured soil moisture values obtained using TRIME-PICO sensors.

At a depth of 10 cm underneath the Vallerani RWH structure the soil moisture peaks regularly (Fig. 17). These peaks can be clearly distuinguished in both the modelled and measured soil moisture values. The peaks of the modelled soil moisture values are higher than the measured values. However, in between the peaks the measured values are higher than the modelled values. At a depth of 30 cm there are less peaks throughout the model period (Fig. 17). Overall the measured and modelled values are very similar in both pattern and magnitude. Except for some of the measured values. These values are higher than the modelled values but are also higher than values measured at a depth of 10 cm.
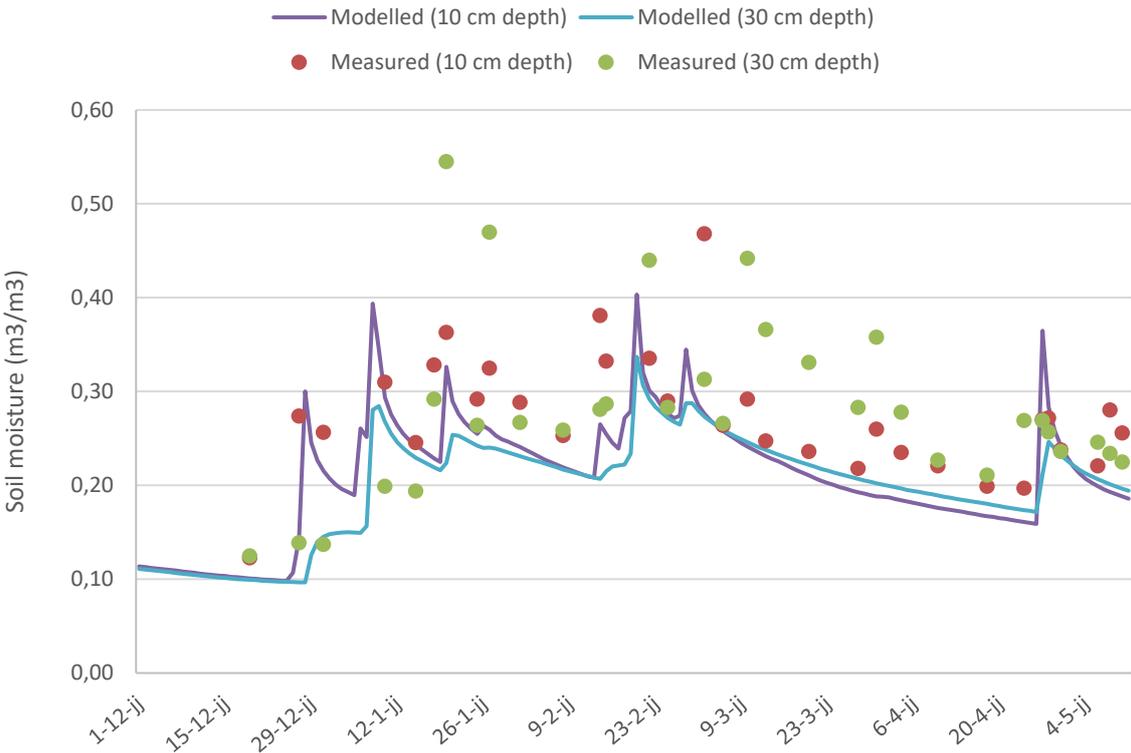
Figure 17 Modelled and measured soil moisture values underneath the furrow of the Vallerani RWH structure at depths of 10cm and 30cm for a period from the 1st of December 2017 till the 5th of May 2018. Measured soil moisture values obtained using TRIME-PICO sensors.

Downstream of the Vallerani RWH structure at a depth of 10 cm the model shows regular peaks (Fig. 18). These peaks are not present in the measured data which shows a steady increase followed by a steady decrease. Except for the peaks, the measured and modelled values are almost equal. At a depth of 30 cm the influence of the infiltration is hardly noticeable and therefore the measured values are steady over the entire period (Fig. 18). The modelled values do not show the same pattern. They clearly peak and are ~4% higher than the measured values.
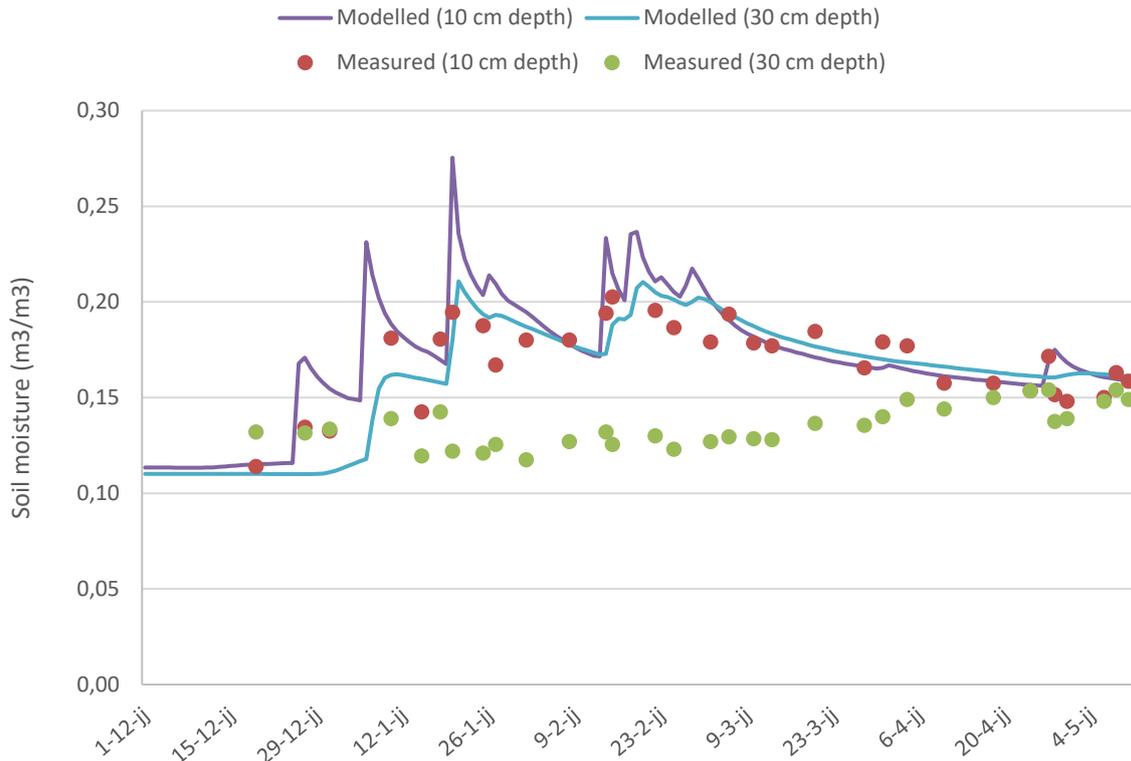
Figure 18 Modelled and measured soil moisture values downstream of the Vallerani RWH structure at depths of 10cm and 30cm for a period from the 1st of December 2017 till the 5th of May 2018. Measured soil moisture values obtained using TRIME-PICO sensors.

4.5 Vallerani RWH structure present day conditions

4.5.1 Potential evapotranspiration

The PET values are the lowest from November till March. For the months January, February and December the PET values are below half a millimeter per day. During the dry summer months, the PET rate peaks at 4.92 mm/day in July. The total PET rate of a year with present day climate conditions is roughly 840 millimeters. This is 7.2 times the amount of annual precipitation. However, during the rainy season the rainfall is 6 times larger than the PET.

4.5.2 Soil moisture dynamics

Figure 19 shows the distribution of soil moisture around the Vallerani RWH structure through time. The 20th of January, the 20th of April and the 20th of July are shown. These are the middle of the rainy season, the end of the rainy season and the expected start of the water stress period, respectively. Halfway through the rainy season most of the soil moisture is still shallow underneath the furrow, the soil moisture is around 27% in this location. Upstream and downstream the precipitation has wetted the surface to ~17%. The ridge stays relatively dry throughout the entire year. At the end of the rainy season the water has had time to percolate deeper into the soil. Because of this the upstream and downstream surface has dried to ~14% moisture content while underneath the furrow it is 17%. The water underneath the furrow has not just percolated but has also distributed in both the upstream and downstream direction. Because of this a band of

25

20-27% moisture content is located at a depth of ~60cm over the entire width of the system. In June this pattern has continued. The water has continued to percolate deeper into the soil and the top of the soil has continued to dry. The band of soil moisture continued to distribute over the system. Because of this the moisture content is ~22% over a larger area.

4.5.3 Water stress
Table 6 gives an overview of the modelled days of water stress the Atriplex Halimus
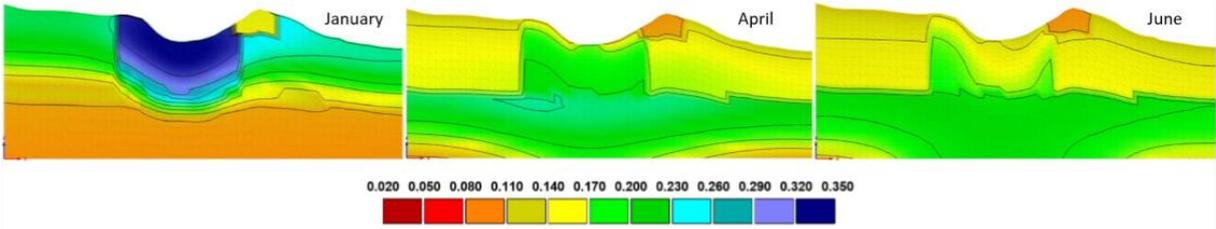
Figure 19 Soil moisture content (m³/m³) under present day climate conditions. Modelled using HYDRUS-2D. The 20th of January, the 20th of April and the 20th of June from left to right.

experiences at various depths and locations. Under present day circumstances, water stress in the Badia under the Vallerani RWH structures is dominant for a large part of the year. The period of water stress starts well after the end of the rainy season, near the end of August. The water stress period continues until the end of December. The soils at a depth of 30cm experience the shortest period of water stress with only 62 days in a year. While at a depth of 10 cm, the period lasts 83 days. The difference is in the start of the water stress period. At a depth of 30 cm, this occurs near the end of September.

The influence of the Vallerani RWH structure on the amount of water stress days is large. Under the interspace the period of water stress in a year is 30-60% longer than under the furrow (Table 6). Underneath the furrow the water stress period is shortest at greater depth. On the interspace the water stress period is longest at greater depths. Vallerani RWH structures allow for the slow infiltration of the water resulting in more water available at greater depths.

Table 6 Days of water stress the Atriplex Halimus experiences in a year. Modelled in the furrow and on the interspace upstream of the furrow.

	Days of water stress	
Depth	**Furrow**	**Interspace**
10	83	120
20	80	151
30	62	161

4.6 Climate scenarios conditions
4.6.1 Precipitation & Surface runoff
The climate scenarios were modelled for an entire year, starting on the 10th of October 2017 and ending on the 9th of October 2018. The precipitation values were reduced with 10, 20 and 30% respectively. The intensity of the rainfall was increased for scenarios 2 and 3.

The decrease in precipitation amount resulted in a decrease in the induced surface runoff (Fig. 20). The sum of the surface runoff in scenario 2 is the lowest. It is 23.7% lower then the surface runoff under present day circumstances. Scenario 2 has less surface runoff than scenario 3 due to the increased intensity of the rainfall. Because of the increased intensity in scenario 3 there is an extra surface runoff event on the 26th of February and on the 26th of April the surface runoff event is larger than for the other scenarios.
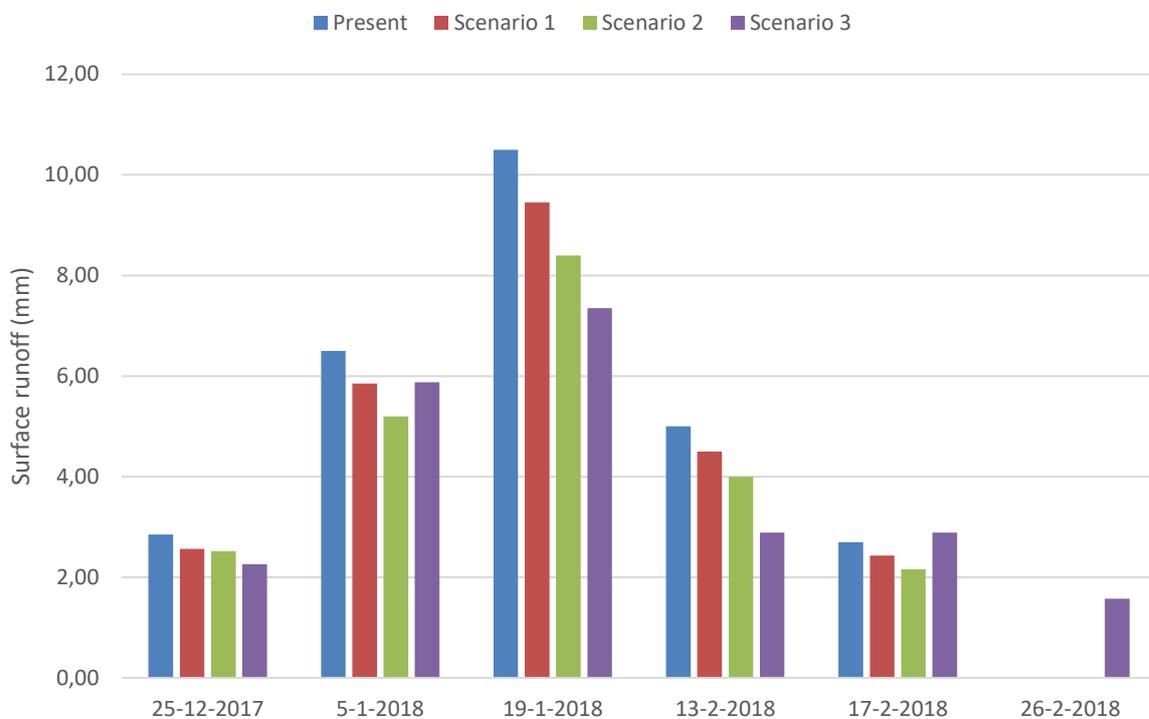
Figure 20 Surface runoff values in the study area for the different scenarios. From 17th of December 2018 till the 20th of April 2018.

4.6.2 Potential evapotranspiration rates
With the increase in temperature of the climate scenarios the PET rates also increase. Table 7 gives an overview of the monthly PET rates for each climate scenario and the present day scenario. The increase in temperature has the biggest impact on the PET rates during the rainy season. With an increase of ~95% between the present day and scenario 3 for January. During the summer months the impact is less noticeable. The increase is only 27% for August between the present and scenario 3.

On an annual basis the increase in PET is noticeable. The aridity index (rainfall divided by PET) of the study area is 0.14 under present day climate conditions. With the increase in PET and the decreased rainfall the region becomes more arid. The aridity indices for the climate scenarios are 0.11; 0.09 and 0.07 respectively. The wet months experience the highest increase in aridity.

Table 7 Overview of the monthly potential evapotranspiration rates.

	Present (mm/day)	Scenario 1 (mm/day)	Scenario 2 (mm/day)	Scenario 3 (mm/day)
January	0.27	0.35	0.44	0.52
February	0.37	0.47	0.58	0.68
March	0.74	0.89	1.06	1.20
April	1.71	1.94	2.22	2.44
May	2.96	3.29	3.67	3.98
June	4.31	4.74	5.22	5.60
July	4.92	5.37	5.88	6.29
August	4.77	5.21	5.70	6.09
September	3.79	4.16	4.58	4.91
October	2.36	2.63	2.94	3.20
November	1.00	1.16	1.35	1.51
December	0.33	0.41	0.52	0.61
Annual total (mm)	841.68	935.75	1043.76	1131.16

4.7 Vallerani RWH structure climate change influence

4.7.1 Soil moisture content

Figure 21 shows the soil moisture content for the different climate scenarios at three times throughout the year. Over time the pattern for each climate scenario is similar to the pattern that is visible under present day circumstances (Fig. 19).

For scenario 1 in January the bulk of the water is concentrated just underneath the furrow, with a moisture content of ~25%. The surface upstream and downstream has been wetted to a moisture content of 16%. In April the surface upstream and downstream has dried to a moisture content of ~13%. Underneath the furrow the moisture content is ~17%. The band that formed in the present situation (Fig. 19) has become less prominent in its size and moisture content. Its moisture content ranges from 18% to 24%.

In January of scenario 2 most of the water is still found underneath the furrow with a moisture content of ~23%. The upstream and downstream surface has wetted to ~15%. In April the drying of the surface has lowered the moisture content to ~12% upstream and downstream. Underneath the furrow the moisture content is 14%. The band has become even less prominent. The total area of the band has become smaller while the water content within the band is only 16-20%. In June the whole system has continued to dry.

With scenario 3 the moisture content underneath the furrow in January is ~20%. In April the drying of the surface has lowered the moisture content to ~11% upstream and downstream. Underneath the furrow the moisture content is ~14%. The band has become less prominent. It does not reach as deep as in previous scenarios and it is also narrower. The moisture content range is 14-18%. In June the band is almost gone due the drying of the soil.
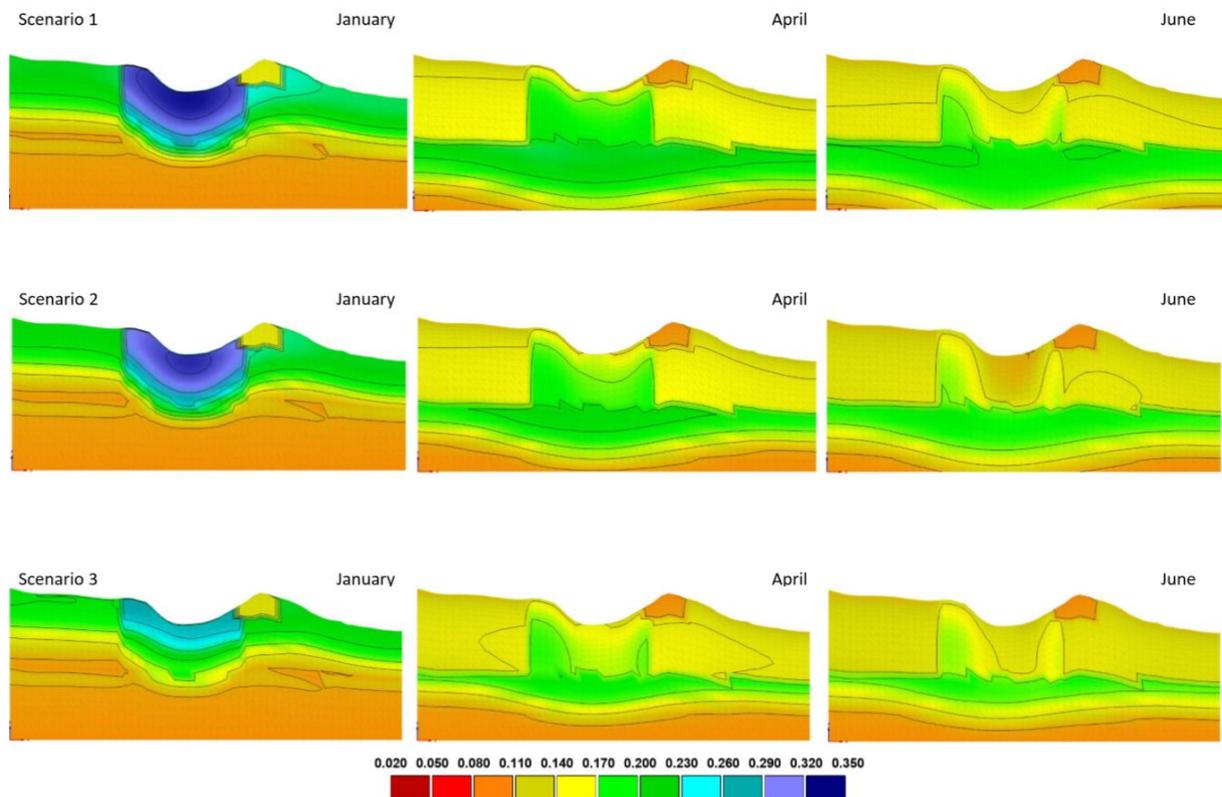
Figure 21 Soil moisture content (m3/m3) under changed climate conditions around a Vallerani RWH structure modelled using HYDRUS-2D. The 20th of January, the 20th of April and the 20th of June from left to right. Climate change scenarios 1-3 from top to bottom.

4.7.2 Water stress

Table 8 gives an overview of the modelled days of water stress the Atriplex Halimus experiences at various depths and under various climate conditions. The period of water stress changes with the change in climate. In scenario 1 the period increases in length with 14-27 days depending on depth. This extra length is a result of the water stress period starting earlier in the year. This trend continues with the other climate scenarios. Climate scenario 2 experiences the longest period of water stress peaking at 125 days.

Depth is an important factor for the water stress. Overall, the least water stress occurs at a depth of 30cm. Under different climate conditions the biggest changes to the water stress period occurs at a depth of 30cm. The increases at a depth of 30 centimeters are 44%, 95% and 71% respectively per climate scenario. While the increases at depths of 10 and 20 centimeters range from 16% to 56%.

Scenario 3 has the lowest amount of rainfall and the highest temperature. However, it has a shorter period of water stress than scenario 2. This is a result of the higher rainfall intensity of scenario 3 compared to scenario 2. The most important factor for the workings of a Vallerani RWH structure is the amount of surface that is induced in the system. A big enough increase in the rainfall intensity can compensate for the lowering of the total rainfall amount and increased temperature.

Table 8 Days of water stress per year underneath the Vallerani RWH structure for each scenario

| Depth | Days of water stress | | | |
	Present	Scenario 1	Scenario 2	Scenario 3
10 cm	83	97	125	101
20 cm	80	95	125	103
30 cm	62	89	121	106

5. Discussion

When Vallerani RWH structures are used to perform water harvesting, the processes on the surface are equally important as the processes in the subsurface. HYDRUS-2D supplies solid capabilities for the modelling of the subsurface processes (Skaggs et al., 2004; Zhou et al., 2007; Sakaguchi et al., 2019). HYDRUS-2D allowed for a lot of flexibility while setting up the model. Different soil textures could be used without restrictions, it supplied a lot of different possibilities for the boundary conditions and rooting zones could be manually placed.

While HYDRUS-2D was found to be more than suitable for the modelling of the subsurface processes, it was found to be severely lacking in its capabilities for modelling the processes on the surface. The rainfall that did not directly infiltrate in to the soil was removed from the system by the software. In reality this excess of rainfall would be the surface runoff that fills up the furrow and slowly infiltrates. It was also not possible to pond water in the model. It had to be forced into the system manually. Simplified calculations were performed outside of the software package to achieve the correct amount of infiltration.

The results that were produced by the model are accurate over a large portion of the studied system. In the top section of the subsurface the model is highly accurate. In the deeper sections of the soil the model is less accurate. The highest inaccuracies are located deeper in the soil. Mostly in the upstream and downstream sections. This is a result of HYDRUS-2D overestimating the lateral flow of water that occurs underneath a Vallerani RWH structure.

The pattern of drying and wetting of the soil is clearly visible in the model results. It takes a large part of the rainy season for the soil to become saturated and it takes several months after the rainy season for the soil to dry. This pattern is in line with findings in the Northern parts of the Badia (Tansey et al., 1999). In general, the arid regions of the northern hemisphere experience this pattern (Ishizuka et al., 2005; Liu et al., 2011; Kolarkar et al., 2018).

At a depth of 30 cm the period of water stress is shorter than in shallower regions. This is due to the percolation of the water to the deeper soils. Ali & Yazar (2007) found that after a rainless period the soil water content, at a depth of 30 cm underneath the furrow, is three times larger than the soil water content just below the surface. While this holds true for the soil directly underneath the furrow little is known about the soil upstream and downstream of the furrow at the same depth. It is unlikely that lateral flow at this depth occurs as is shown by the model. The lateral flow is relatively equal in both the upstream and downstream direction while in reality it is likely more prominent in the downstream direction due to gravity.

The construction of Vallerani RWH structures positively influences the amount available water for the Atriplex Halimus planted in the furrow. On the interspace between two Vallerani RWH structures the Atriplex Halimus experiences almost two times the amount of water stress compared to the furrow. The shortest period of water stress is experienced at a depth of 30cm underneath the furrow. Atriplex Halimus roots reach deep enough into the soil to be able to withdraw water from this depth.

If an Atriplex Halimus seedling is affected by water stress it will severely hampered in its growth (Hassine & Lutts, 2010). However, Atriplex Halimus that has had time to grow will have a better resistance to water stress (Martìnez et al., 2004). Therefore, the Atriplex Halimus should be grown under regulated conditions before being transplanted into the Vallerani RWH structures. The ideal shrub age before transplanting is 4-5 months (Al-Satari et al., 2018). The ideal time to transplant the shrubs would be in December. At that time no water stress is present and it allows the longest unhindered growth period or the Atriplex Halimus.

The pattern of the soil moisture around a Vallerani RWH structure remains the same when influenced by climate change. However, the total amount of soil moisture in the system is lower. The impact of climate change on the water availability is most noticeable at greater depths. Due to the lowering of soil moisture in the system there is an increase in the days of water stress experienced by the Atriplex Halimus. This increase is most severe at the greater depths. The period of water stress experienced by the Atriplex Halimus can potentially double. This will influence the growing potential of this shrub type. Studies have been performed to test the effects of water stress on Atriplex Halimus. However, these studies only expose the shrub to a maximum of 27 days of consecutive water stress (Martìnez et al., 2004; Hassine & Lutts, 2010). These studies show that the shorter periods of water stress have a limited effect on the Atriplex Halimus. However, the model indicates that the period of water stress could reach up to 125 days. Therefore, new research into the survivability of Atriplex Halimus for longer periods of water stress is recommended.

The climate scenarios used in this study are relatively simple scenarios. Rainfall amount decrease, temperature increase and rainfall intensity increase are the three climate change factors that are focused on. While these are the main three factors that will be altered due to climate change (Kunstmann et al., 2007; Evans, 2009; Lelieveld et al., 2012) the exact degree with which each of these factors will change is still unknown. The results have shown that the most important factor for the Vallerani RWH structure regarding climate change is the rainfall intensity. Therefore, it is important to study the exact nature of how these three factors change to be able to assess the influence of climate change on the water retention capacity of the Vallerani RWH structures.

6. Conclusion

The Jordanian Badia has experienced a high amount land degradation in the past decades as a result of poor land management. To stop the land degradation and improve the resilience of the ecosystem, Vallerani RWH structures were constructed. This study focused on the impact of these Vallerani RWH structures on the soil moisture and the viability of the structures regarding climate change.

HYDRUS-2D was used to model the soil moisture dynamics surrounding a Vallerani RWH structure. Fieldwork was performed to calibrate and evaluate the model. A model with a Kling-Gupta efficiency of 0.55 was created. This model showed that the structures had a positive influence on the water availability in the soil underneath the Vallerani RWH structure. The surface runoff is caught by the furrow and has time to infiltrate. As a result of the slow infiltration of the surface runoff the Atriplex Halimus experiences only half of the water stress compared to the interspace.

Climate change will have a negative impact on the water available to the shrubs growing in the Vallerani RWH structure. For this study climate change was simulated by changing three factors: the rainfall amount (decrease), the temperature (increase) and the rainfall intensity (increase). The rainfall intensity is the most important of these factors on the workings of the Vallerani RWH structure. The increased surface runoff as a result of the increase in rainfall intensity can (over)compensate for the lowering of the rainfall amount and the increase temperature. How much impact the climate change will have on the capacity of vegetation growth in the Vallerani RWH structures depends on the degree with which each of the three climate factors will change over time.

References

Akroush, S., Shideed, K., & Bruggeman, A. (2011). Adaption, environmental impact and economic assessment of water harvesting practices in the Badia benchmark site. *Water Benchmarks of CWANA*, 161-175.

Ali, A., & Yazar, A. (2007). *Effect of Micro-catchment Water Harvesting on Soil-water Storage and Shrub Establishment in the Arid Environment.*

Ali, A., Development Bank, A., & Bruggeman, A. (2006). *The Vallerani Water Harvesting System Flood damage and need assessment View project International Platform for Drylands Research and Education View project SEE PROFILE.*

Al-Satari, Y., Al-Dein Al-Ramamneh, E., Ayad, J., Dalbouh, M., Amayreh, I., & Khreisat, Z. (2018). Impact of seedling age on the survival and productivity of Atriplex halimus shrubs in drought-affected rangelands of Jordan. *Rangeland Journal, 40*(3), 287-296.

Belkheiri, O., & Mulas, M. (2013, 2). The effects of salt stress on growth, water relations and ion accumulation in two halophyte Atriplex species. *Environmental and Experimental Botany, 86*, 17-28.

Chávez, J., & Evett, S. (2012). *USING SOIL WATER SENSORS TO IMPROVE IRRIGATION MANAGEMENT.*

Dingman, S. (2015). *Physical Hydrology* (Third ed.). Waveland press inc.

El Kharraz, J., El-Sadek, A., Ghaffour, N., & Mino, E. (2012). Water scarcity and drought in WANA countries. *Procedia Engineering.*

Evans, J. (2009, 2). 21st century climate change in the Middle East. *Climatic Change, 92*(3-4), 417-432.

FAO. (2018). *FAOSTAT*. Retrieved from http://www.fao.org/faostat/en/#home

Fukai, S. (2019). *Effect of micro-catchment water harvesting on soil moisture condition in Jordan's Badia.* The United Graduate School of Dryland Science, Tottori.

Gupta, H., Kling, H., Yilmaz, K., & Martinez, G. (2009, 10 20). Decomposition of the mean squared error and NSE performance criteria: Implications for improving hydrological modelling. *Journal of Hydrology, 377*(1-2), 80-91.

Haddad, M. (2019). *Exploring Jordan's rangeland transition: Merging restoration experiment with modeling - A case study from Al Majdiyya village.* Faculty of Graduate Studies, The University of Jordan, Amman.

Hassine, A., & Lutts, S. (2010, 11 15). Differential responses of saltbush Atriplex halimus L. exposed to salinity and water stress in relation to senescing hormones abscisic acid and ethylene. *Journal of Plant Physiology, 167*(17), 1448-1456.

Hopmans, J., Šimůnek, J., Romano, N., & Durner, W. (2002). *Inverse Modeling of Transient Water Flow* (Third ed.). (J. H. Dane and G. C. Topp, Ed.) Madison: SSSA.

Ishizuka, M., Mikami, M., Yamada, Y., Zeng, F., & Gao, W. (2005, 9 27). An observational study of soil moisture effects on wind erosion at a gobi site in the Taklimakan Desert. *Journal of Geophysical Research D: Atmospheres, 110*(18), 1-10.

Kling, H., Fuchs, M., & Paulin, M. (2012, 3 6). Runoff conditions in the upper Danube basin under an ensemble of climate change scenarios. *Journal of Hydrology, 424-425*, 264-277.

Kolarkar, A., Murthy, K., & Singh, N. (2018, 10 1). 'Khadin—A method of harvesting water for agriculture in the Thar Desert. *Journal of Arid Environments, 6*(1), 59-66.

Kunstmann, H., Suppan, P., Heckl, A., & Rimmer, A. (2007). *Quantification and Reduction of Predictive Uncertainty for Sustainable Water Resources Management.* IAHS Publ.

Lelieveld, J., Hadjinicolaou, P., Kostopoulou, E., Chenoweth, J., El Maayar, M., Giannakopoulos, C., . . . Xoplaki, E. (2012, 10). Climate change and impacts in the Eastern Mediterranean and the Middle East. *Climatic Change, 114*(3-4), 667-687.

Liu, Y., Parinussa, R., Dorigo, W., De Jeu, R., Wagner, W., M. Van Dijk, A., . . . Evans, J. (2011). Developing an improved soil moisture dataset by blending passive and active microwave satellite-based retrievals. *Hydrology and Earth System Sciences, 15*(2), 425-436.

Malagnoux, M. (2008). Degraded Arid Land Restoration for Afforestation and Agro-Silvo-Pastoral Production through New Water Harvesting Mechanized Technology. *The Future of Dry Lands*, 269-282.

Marra, W. (2016). Orthophoto and DEM generation from UAV -imagery using Structure -from - Motion with AgiSoft Photoscan.

Martìnez, J., Ledent, J., Bajji, M., Kinet, J., & Lutts, S. (2003). Effect of water stress on growth, Na+ and K+ accumulation and water use efficiency in relation to osmotic adjustment in two populations of Atriplex halimus L. *Plant Growth Regulation*.

Mualem, Y. (1976). *A New Model for Predicting the Hydraulic Conductivity of Unsaturated Porous Media.*

Mudabber, M., Oweis, T., Suifan, M., Shawahneh, N., Sattar, Y., Ziadat, F., . . . Karrou, M. (2011). Effect of water harvesting techniques on water productivity and soil erosion. *Water Benchmarks of CWANA*, 29-55.

Oweis, T., & Hachum, A. (2006). Water harvesting and supplemental irrigation for improved water productivity of dry farming systems in West Asia and North Africa. *Agricultural Water Management, 80*(1-3 SPEC. ISS.), 57-73.

Oweis, T., Prinz, D., & Hachum, A. (2013). Water harvesting; indigenous Knowledge for the future of the drier environments. *Journal of Chemical Information and Modeling, 53*(9), 1689-1699.

Photo, U., & Dormino, M. (2018). *Sustainable Development Goal 6 Synthesis Report on Water and Sanitation 2018 Sustainable Development Goal 6 Synthesis Report on Water and Sanitation.*

Sakaguchi, A., Yanai, Y., & Sasaki, H. (2019, 6 20). Subsurface irrigation system design for vegetable production using HYDRUS-2D. *Agricultural Water Management, 219*, 12-18.

Schaap, M., Leij, F., & van Genuchten, M. (1998, 7 27). Neural Network Analysis for Hierarchical Prediction of Soil Hydraulic Properties. *Soil Science Society of America Journal, 62*(4), 847.

Schaap, M., Leij, F., Van Genuchten, M., & Brown, G. (2001). rosetta: a computer program for estimating soil hydraulic parameters with hierarchical pedotransfer functions. *Journal of Hydrology, 251*, 163-176.

Šimůnek, J., & Hopmans, J. (2002). *Parameter Optimization and Nonlinear Fitting* (Third ed.). (J. H. Dane and G. C. Topp, Ed.) Madison: SSSA.

Šimůnek, J., Jacques, D., Hopmans, J., Inoue, M., Flury, M., & van Genuchten, M. (2002). *Solute Transport During Variably-Saturated Flow - Inverse Methods* (Third ed.). (J. H. Dane and G. C. Topp, Ed.) Madison: SSSA.

Šimůnek, J., Van Genuchten, M., & Šejna, M. (2008). *Numerical Modelling of Hydrodynamics for Water Resources-Garcia-Navarro & Playán (eds).*

Singh, J., Lo, T., Rudnick, D., Dorr, T., Burr, C., Werle, R., . . . Muñoz-Arriola, F. (2018, 1 31). Performance assessment of factory and field calibrations for electromagnetic sensors in a loam soil. *Agricultural Water Management, 196*, 87-98.

Skaggs, T., Trout, T., Šimůnek, J., & Shouse, P. (2004, 7 16). Comparison of HYDRUS-2D Simulations of Drip Irrigation with Experimental Observations. *Journal of Irrigation and Drainage Engineering, 130*(4), 304-310.

Slatyer, R. (1970). Comparative photosynthesis, growth and transpiration of two species of Atriplex. *Planta*.

Sona, G., Pinto, L., Pagliari, D., Passoni, D., & Gini, R. (2014). Experimental analysis of different software packages for orientation and digital surface modelling from UAV images. *Earth Science Informatics*.

Strohmeier, S. (2019). Email.

Strohmeier, S., Haddad, M., Vries, J., Saba, M., Obeidat, E., & Nouwakpo, S. (2018). Restoring Degraded Rangelands in Jordan: Optimizing Mechanized Micro Water Harvesting Technique Using Rangeland Hydrology and Erosion Model (RHEM). World Conference Soil and Water Conservation Under Global Change (CONSOWA).

Tansey, K., Millington, A., Battikhi, A., & White, K. (1999, 10). Monitoring soil moisture dynamics using satellite imaging radar in northeastern Jordan. *Applied Geography, 19*(4), 325-344.

UNCCD, S. (2017). Policy Brief No. 3: Sustainable Land Management Solutions.

Van Genuchten, M. (1980). A Closed-form Equation for Predicting the Hydraulic Conductivity of Unsaturated Soils 1. *Soil Science Society of America Journal, 44*, 892-898.

Van Genuchten, M. (1985). Convective-dispersive transport of solutes involved in sequential first-order decay reactions. *Computers and Geosciences*.

Vörösmarty, C., McIntyre, P., Gessner, M., Dudgeon, D., Prusevich, A., Green, P., . . . Davies, P. (2010). Global threats to human water security and river biodiversity. *Nature*.

Wenhao, F. (2001). Control work in close range photogrammetry. *Geo-Spatial Information Science*.

Zhou, Q., Kang, S., Zhang, L., & Li, F. (2007, 2). Comparison of APRI and Hydrus-2D models to simulate soil water dynamics in a vineyard under alternate partial root zone drip irrigation. *Plant and Soil, 291*(1-2), 211-223.

Ziadat, F., Bruggeman, A., Oweis, T., Haddad, N., Mazahreh, S., Sartawi, W., & Syuof, M. (2012, 10). A Participatory GIS Approach for Assessing Land Suitability for Rainwater Harvesting in an Arid Rangeland Environment. *Arid Land Research and Management, 26*(4), 297-311.

Appendix A

Inverse parameter estimation modelling

A total of 12 inverse model runs were performed and completed. Eight of these twelve runs resulted in soil parameters. These eight parameters sets were used to further run the model. The inverse model runs differed on the used amount of sensors. Ranging from all ten sensors to as low as two sensors. Table 1 gives an overview of the inverse modelling runs and the results. The inverse modelling was not a smooth process. Low amount of iterations was performed, on average two per parameter set. Values would go out of realistic boundaries to fit the input data. Only parameter set 2 gave a reasonable KGE for the deep lying sensors. However due to its unrealistic performance within the top half of the model it was deemed unsuitable. Due to the lack of good results of the inverse modelling, poor performance of the Decagon sensors and lack of measurements with the TRIME-PICO sensors it was deemed impossible to successfully model the soil moisture dynamics surrounding the Vallerani RWH structure using this method.

Table 1 Overview and GOF of the finished inverse modelling runs.

| Inverse parameter set	Sensors used for inverse model	r (-)	BIAS (%)	KGE (-)	r - 30cm depth (-)	BIAS - 30cm depth (%)	KGE - 30cm depth (-)
1	All sensors	0.24	-0.2	0.21	0.52	23.4	0.2
2	Sensors UV and DS	0.34	-10	0.08	0.62	-0.4	0.49
3	Sensors UV and lose soil	0.21	-11.4	-0.07	0.12	-14.2	-0.03
4	Sensors UV	0.21	-11.7	-0.08	0.12	-13.9	-0.05
5	Sensors UV, DS and lose soil	0.25	1.3	0.24	0.54	25.5	0.13
6	Sensors UV and lose soil + soil restriction	0.41	-12.7	0.07	0.7	-7.7	0.35
7	Sensors UV, DS and lose soil + soil restriction	0.3	42.7	0.18	0.46	28.3	0.2
8	All sensors + soil restriction	0.11	-2.1	-0.02	0.43	0.3	0.35

Appendix B

Photogrammetry

Photogrammetry is the science of creating a 3-D surface from 1-D images. These images have to be taken along an object with an overlap of at least 60%. Just like the human brain, photogrammetry creates a 3-D surface by comparing the overlap of both individual images (Marra, 2016). Traditionally photogrammetry uses photos taken from an airplane. However, as a result of technological advancements it has become more common for the data to be provided by commercial grade cameras on UAVs (Unmanned Airborne Vehicles).

With the technological advancements in the past decade's close-range photogrammetry has become a viable and cheap option to obtain data. Using close-range photogrammetry, a surface was created for one of the Vallerani structures in the test site. This was done by taking photos along each side of the structure with a suitable overlap of at least 70%. To turn these photos into a 3D surface it was necessary to set up a coordinate system for the structure. Three methods exist to generate a coordinate system around the structures. These methods can be used separately or together (Wenhao, 2001). Method one is the use of ground control points. At least three points are required to get a coordinate system (Wenhoa, 2001). Method two assigns values to one of the images. When this is done the coordinate net can be drawn using known lengths between objects surrounding and including the Valleranis (Wenhao, 2001). The third method assigns values for an object space point. Then according to the relative control of object space line the coordinate net can be concluded (Wenhao, 2001). For this study ground control points were used. Surrounding the Vallerani structure clearly recognisable and distinguishable markers were placed that can be recognised on multiple images. Using these markers, the coordinate system can be created.

When the photos were taken and the coordinate system was set up the data was imported into Agisoft Photoscan Professional. Present day this is the best software for photogrammetry (Sona et al., 2014). However, it is a black box software so the workings are vague. Within this software the images will be put through several steps to generate the 3D surface (Fig. 1). The first step is pattern recognition. During this the software will be able to match overlapping images. The second step is manually setting up the control point markers in all the images. Doing this will greatly increase the accuracy of the overlapping images. With these
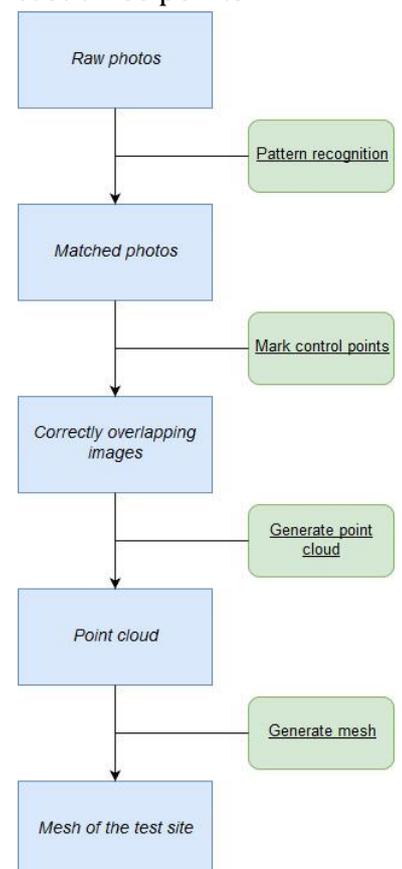
Figure 1 The Agisoft workflow to create a mesh from photos.

accurately overlapping images the software can generate a point cloud. Using this point cloud, a mesh can be generated.

Appendix C

Model setup
Material distribution
Seven different materials were used in the model (Table 1).

- Material 1: Shallow material underneath shrub basin
- Material 2: Surface crust outside the furrow
- Material 3: Material with a depth of ~70 cm
- Material 4: Surface crust inside the shrub basin
- Material 5: Less compacted soil in the ridge
- Material 6: Shallow material downstream of the shrub basin
- Material 7: Shallow material upstream of the shrub basin

Tabel 1 The Van Genuchten parameters for every material used in the final model run.

Material	Q_r	Q_s	Alpha	n	K_s	I
	(-)	(-)	(1/cm)	(-)	(cm/day)	(-)
1	0.0861	0.466	0.0086	1.5164	17.5	0.5
2	0.0548	0.291	0.0188	1.2093	0.6	0.5
3	0.0952	0.490	0.0113	1.4246	15.8	0.5
4	0.0709	0.363	0.0108	1.3719	2.1	0.5
5	0.0885	0.180	0.0087	1.5154	30.3	0.5
6	0.0861	0.350	0.0086	1.5154	17.0	0.5
7	0.0861	0.320	0.0086	1.5154	17.0	0.5

Root distribution
The roots are located in the middle of the shrub basin with a spread of roughly 25 cm in the upstream and downstream direction. The depth of the roots is set to 45 cm over the entire width. The root uptake magnitude of the roots is set equal over the entire root area.

Boundary conditions
Four different boundary conditions are used to set up the model.

- Free drainage is used at the lower boundary and the downstream boundary. This allows for water to leave the system if the option exist.
- No flux is used at the upstream boundary. No water flow should occur over this boundary.
- The atmospheric boundary is applied over the entire surface except for a small gap where Variable flux 1 is placed. This boundary results in precipitation, transpiration and evapotranspiration successfully occurring along the top of the model.

- Variable flux 1 is used at the centre of the furrow with a spread of ~9 cm upstream and downstream. This boundary allows for the forced infiltration of water.

Initial conditions

The initial conditions were setup to be similar to the conditions after the summer months. The water content at the top of the system was set to 12% with a linear distribution to 10% at the bottom.

Observation points

Observation points serve two purposes. For the inverse modelling part of the modelling they were used to feed the inverse modelling data into the model. For the other model runs it is the location modelled values can be exported from. Therefore, the observation nodes were placed to simulate the placement of the real life sensors.